Magnetization of the spin-$\frac{1}{2}$ Heisenberg antiferromagnet on the triangular lattice

Qian Li,[1,2] Hong Li,[3] Jize Zhao,[1,2,*] Hong-Gang Luo,[1,2,4] and Z. Y. Xie[3,†]

[1]*School of Physical Science and Technology & Key Laboratory for Magnetism and Magnetic Materials of the MoE, Lanzhou University, Lanzhou 730000, China*

[2]*Lanzhou Center for Theoretical Physics and Key Laboratory of Theoretical Physics of Gansu Province, Lanzhou University, Lanzhou 730000, China*

[3]*Department of Physics, Renmin University of China, Beijing 100872, China*

[4]*Beijing Computational Science Research Center, Beijing 100084, China*

(Received 24 February 2022; accepted 5 May 2022; published 16 May 2022)

After decades of debate, now there is a rough consensus that at zero temperature the spin-1/2 Heisenberg antiferromagnet on the triangular lattice is three-sublattice 120° magnetically ordered, in contrast to a quantum spin liquid as originally proposed. However, there remains considerable discrepancy in the magnetization reported among various methods. To resolve this issue, in this work we revisit this model by the tensor-network state algorithm. The ground-state energy per bond E_b and magnetization per spin M_0 in the thermodynamic limit are obtained with high precision. The former is estimated to be $E_b = -0.18334(10)$. This value agrees well with that from the series expansion. The three-sublattice magnetic order is firmly confirmed and the magnetization is determined as $M_0 = 0.161(5)$. It is about 32% of its classical value and slightly below the lower bound from the series expansion. In comparison with the best estimated value by Monte Carlo and density-matrix renormalization group, our result is about 20% smaller. This magnetic order is consistent with further analysis of the three-body correlation. Our work thus provides benchmark results for this prototypical model.

DOI: 10.1103/PhysRevB.105.184418

I. INTRODUCTION

One challenging task in modern condensed matter physics is to search for exotic states of matter both experimentally and theoretically. In this long journey, systems with geometric frustration have emerged as a flourishing research area. In usual magnets, spins freeze into some periodic patterns upon cooling, associated with a phase transition from a paramagnetic phase to an ordered phase. The transition temperature, in comparison with the Curie-Weiss temperature, may be drastically suppressed by geometric frustration. Actually, in 1973, Anderson already proposed that some frustrated magnets may remain disordered even at zero temperature, which is now known as the quantum spin liquid [1–5]. Ever since then, a large amount of interest has been attracted to search for such exotic states [6,7]. Particularly, in Anderson's original paper [1], the spin-1/2 antiferromagnetic Heisenberg model on the triangular lattice (TAHM) was conjectured to be such a candidate. Moreover, Anderson proposed that its ground state may be a resonating valence-bond state (RVB) rather than a state with three-sublattice 120° magnetic order (TMO) in its classical counterpart.

In the past decades, to clarify the nature of its ground state, TAHM has been extensively studied by a variety of analytical and numerical methods [8–30]. For example, Huse and Elser examined this model by variational Monte Carlo [8]. They chose a trial wave function with three-spin terms. By comparing its ground-state energy with that of RVB-type wave functions, they found that the former is energetically favored, and its magnetization is finite, about 68% of its classical value. On small clusters, exact diagonalization (ED) calculations were performed by several groups but their conclusions are conflicting [11–14]. The Green's function Monte Carlo (GFMC) [15] and density-matrix renormalization group (DMRG) [16] calculations, which were on moderate clusters, concluded the existence of an ordered ground state with a consistent magnetization $M_0 \approx 0.205$. As far as we know, so far the smallest but finite magnetization reported is $M_0 = 0.1625(30)$, obtained by GFMC with fixed node approximation [17]. Now it is mostly believed that the ground state of the TAHM is a TMO state with strongly suppressed magnetization.

However, whereas such progress has been made, the debate has never ceased completely so far. For example, recent numerical analyses based on bold diagrammatic Monte Carlo [18] and ED [14] supported the absence of magnetic order. Moreover, even in those works supporting the existence of TMO, the discrepancy of the magnetization is quite large, with its value ranging from 0.1625(30) to 0.36 [17,19]. And finally, from the experimental perspective, various compounds with triangular geometry have been synthesized and fingerprints of quantum spin liquids were reported [31,32], but their nature remains controversial. As a prototypical model with geometric frustration, precise understanding of the TAHM is important and necessary. In particular, an accurate estimate of the magnetization may help us to understand related

*zhaojz@lzu.edu.cn
†qingtaoxie@ruc.edu.cn

experiments and serve as a benchmark for newly developed numerical algorithms. It is fair to say that the present knowledge remains unsatisfactory and thus calls for further studies on this model.

For this purpose, we revisit this model by the tensor-network state (TNS) method [33–37], which is under rapid development and has drawn great attention due to its successful applications in strongly correlated condensed matter physics [38–40], statistical physics [41–43], quantum field theory [44–46], machine learning [47,48], etc. To be specific, the TAHM is described by the Hamiltonian

$$\mathcal{H} = J \sum_{\langle ij \rangle} \hat{\mathbf{S}}_i \cdot \hat{\mathbf{S}}_j, \tag{1}$$

where $J > 0$ is the antiferromagnetic coupling. Hereafter we set $J = 1$ as the energy unit. $\hat{\mathbf{S}}_i$ is the spin operator at site i. $\langle \cdots \rangle$ means a summation over the nearest-neighbor pairs. We use the projected entangled simplex state (PESS) ansatz [49] to represent the ground-state wave function and employ the corner transfer-matrix renormalization group (CTMRG) method [39,50,51] to estimate the physical quantities, such as E_b, M_0, and many-body correlation [52].

The rest of the paper is organized as follows. In Sec. II, we introduce some details of the algorithm employed in our work. The numerical results for E_b, M_0, and many-body correlation are present in Sec. III. In Sec. IV, we summarize our work.

II. METHODS

Frustration in TAHM makes it difficult to be investigated with traditional numerical methods such as Monte Carlo, which suffers from the infamous sign problem and strong finite-size effect. Generally, the TNS method is free of the sign problem and can study this model in the thermodynamic limit directly by assuming a translationally invariant wave function. Therefore, it is drawing increasing attention nowadays.

In the TNS family, PESS is a wave function ansatz [49] generalized from the popular projected entangled pair state (PEPS) ansatz [35] and is believed to be suitable for frustrated systems. In this work, the PESS ansatz is defined as

$$|\Psi\rangle = \sum_{\{\sigma\}} \mathrm{Tr}\big(\ldots S^{(\mu\nu)}_{i_{\mu\nu} j_{\mu\nu} k_{\mu\nu}} A^{(\lambda\omega)}_{i_{\lambda\omega} j_{\lambda\omega} k_{\lambda\omega}} [\sigma_{\lambda\omega}] \ldots\big) | \ldots \sigma_{\lambda\omega} \ldots \rangle, \tag{2}$$

which is illustrated in Fig. 1. Here (μ, ν) denotes the location of the upward triangles and (λ, ω) denotes the location of the lattice sites. A rank-3 simplex tensor S is defined at the center of each upward triangle and a rank-4 projection tensor A is defined at each lattice site. $\{i, j, k\}$ and $\{\sigma\}$ are the virtual indices and physical basis associated with the tensors, respectively. The two virtual indices associated with the same bond take the same values. Tr is over all the repeated virtual indices and $\sum$ is over all the basis configurations.

To employ the translational invariance, we use a 3×3 periodicity, which means that

$$S^{(\mu,\nu)} = S^{(\mu+3m,\nu+3n)}, \quad A^{(\lambda,\omega)} = A^{(\lambda+3m,\omega+3n)}, \tag{3}$$

where m, n are integers. In other words, we totally have nine different S and nine different A in the ansatz (2). The corresponding unit cell is illustrated by a dashed rhombus in Fig. 1.

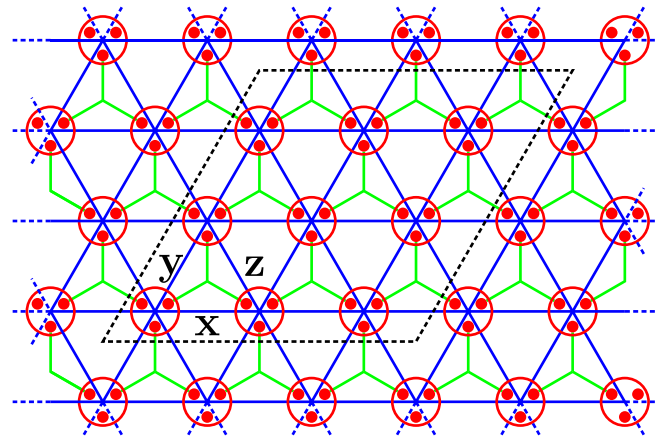

FIG. 1. Schematic diagram of the PESS wave function ansatz on the infinite triangular lattice. The blue lines are the bonds of the lattice, which are marked by x, y, and z, respectively. The green lines represent virtual bonds of the wave function. The tensors sitting at the center of the triangles are the simplex tensors S and the tensors covered by red circle are the projection tensors A. The rhombus with dashed lines marks a 3×3 unit cell of the trial wave function. The physical indices are perpendicular to the plane and not shown here.

It is known that the bond dimension, D, which is the maximal value of the virtual indices, controls the number of independent parameters and thus the numerical accuracy. In this work, D is up to 13. The ground-state wave function is optimized by a simple update algorithm [53,54]. Though the full update strategy [55] might be more accurate, it is much more costly. To verify the result, we compared the magnetizations at $D = 6$ so that the full update and the recent automatic differentiation [56] can be performed. The simple update approach gives an estimation of about 0.2448. Starting from such a wave function, full update and automatic differentiation [57] can further reduce the magnetization down to 0.2395 and 0.2382, respectively. The difference among these results is of the order 10^{-3}. In viewing the computational cost, we choose the more efficient simple update scheme in this work. The numerical accuracy can be remedied by larger D. In order to avoid the bias and reduce the Trotter error, we started from a wave function randomly generated in complex field and gradually reduced the Trotter step τ from a large value, say 0.2. The final τ is smaller than 10^{-3}, which turns out to be sufficiently small to estimate the magnetization of TAHM.

Physical observables are calculated via the CTMRG method, which was developed for an arbitrary unit cell on the square lattice [39]. In Fig. 1, we show the PESS ansatz defined on a honeycomb skeleton. First, we formally deform the skeleton to a square by simply combining S with A together to form a single tensor T, e.g.,

$$T^{(\mu\nu)}_{k_1 k_2 i_1 i_2}[\sigma] = \sum_j S^{(\mu\nu)}_{i_1 j k_1} A^{(\mu,\nu+1)}_{i_2 j k_2}[\sigma]. \tag{4}$$

This is done in all the upward triangles coherently, as illustrated in Fig. 2(a). Hence the reduced network $\langle \Psi | \Psi \rangle$, which appears in expectation value calculation, see Eqs. (5) and (6), can be represented as a two-dimensional tensor network with a 3×3 periodicity, as illustrated in Fig. 2(b), and then

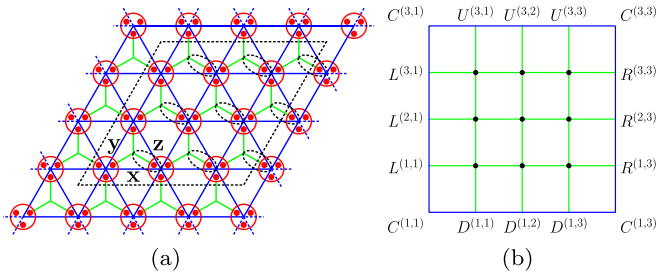

FIG. 2. (a) Converting the tensor network skeleton from the honeycomb lattice to a square lattice by one-step contraction, e.g., in the direction of the bonds surrounded by dashed ellipses. (b) The 3×3 unit cell obtained after deformation in the reduced network $\langle\Psi|\Psi\rangle$. Here the environment tensors of the unit cell are shown explicitly, e.g., $L^{(3,1)}$ are the edge tensors associated with the left of $T^{(3,1)}$.

the standard CTMRG method can be applied directly to contract the network. Finally, the local physical observables can be calculated efficiently from the local environment tensors $\{L, R, U, D, C\}$. Similarly, the bond dimension χ of the environment tensors is a tunable parameter which controls the accuracy in CTMRG. In our calculation, the maximal χ is no less than D^2 to ensure a reliable result [58].

III. RESULTS

A. Ground-state energy

The ground-state energy usually serves as a key criterion for trial wave functions, particularly in the variational Monte Carlo simulations. This is exactly how Huse and Elser excluded the quantum spin liquid ground state in TAHM [8]. From this aspect, an accurate estimate of the ground-state energy is important. Therefore, first we need to check whether our numerical results are reliable, by comparing the ground-state energy with that in previous works.

The ground-state energy for a given bond $\langle ij\rangle$ is given by

$$E_{\langle ij\rangle} = \frac{\langle\Psi|\hat{\mathbf{S}}_i \cdot \hat{\mathbf{S}}_j|\Psi\rangle}{\langle\Psi|\Psi\rangle}, \tag{5}$$

where $|\Psi\rangle$ is the PESS representation of the ground-state wave function; see Eq. (2). Since our system is translationally invariant, the bond energy E_b can be estimated by averaging $E_{\langle ij\rangle}$ over all bonds in one unit cell.

As stated in the previous section, the accuracy of the wave function is controlled by D and that of the expectation is controlled by χ. Therefore, to obtain accurate results for a given D, the expectation values are calculated with a series of χ in which the largest one is no less than D^2 and then extrapolated as $\chi \to \infty$.

For the smallest $D = 4$ in our simulations, the ground-state energy is $E_b = -0.18226(9)$, which is already lower than that obtained by GFMC [15], $-0.18193(3)$, and is also lower than that obtained by the infinite-PEPS calculation whose ansatz is defined on the decorated square latice [59] with $D = 4$, -0.1813. To provide an intuitive impression, in Fig. 3, we plot E_b as a function of $1/\chi$ for $D = 10,\ 11,\ 12$, and 13. It seems that E_b depends very weakly on D when χ becomes large and all the data points are well below those from GFMC.

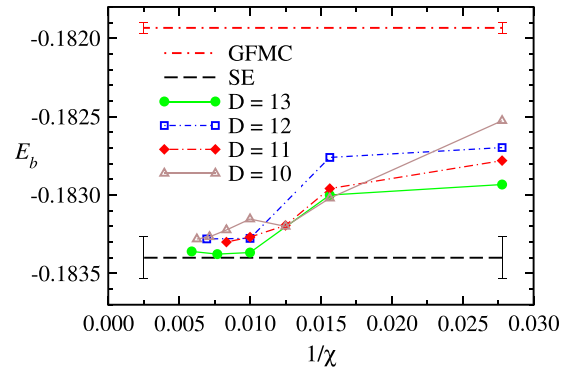

FIG. 3. Ground-state energy E_b for $D = 10,\ 11,\ 12$, and 13 is plotted as a function of χ. The numerical error is on the fifth digit and they are not shown for a clear vision. The data obtained by GFMC [15] and SE [21] are also shown for comparison. Our data are obviously below that from GFMC but agree well with that by SE (within the error bar).

As χ increases, E_b roughly decreases monotonically, but they oscillate in a small interval as a function of D. For the data points with largest χ in Fig. 3, E_b is between -0.18328 and -0.18336. With the available χ, this nonmonotonic behavior with regard to D makes it difficult to extrapolate our data and hinder us to obtain more accurate results. As a compromise, we first extrapolate the data for $D = 10,\ 11,\ 12$, and 13 to the infinite χ limit, respectively, and then average them. Our final result is $E_b = -0.18334(10)$, which agrees well with that obtained by the series expansion (SE) [21] and the coupled cluster method [28].

In Table I, we summarize some recent works for comparison. These data indicate that our PESS wave function represents a good approximation of the ground state of TAHM.

B. Magnetization

The main debate about this model is whether the ground state is a TMO state or a quantum spin liquid. From Table I, we can see that, even in those works advocating TMO, the magnetization M_0 differs significantly. For example, if the error bar is taken into account, the low bound given by SE [26] is smaller than half of that given in Ref. [19]. This motivates us to calculate the magnetization in this work. Given the ground state $|\Psi\rangle$, three components of the magnetization vector $\vec{M}_i$ at the site i are given by

$$M_i^\alpha = \frac{\langle\Psi|\hat{\mathbf{S}}_i^\alpha|\Psi\rangle}{\langle\Psi|\Psi\rangle}, \quad \alpha = x, y, z, \tag{6}$$

from which the magnetization at site i reads

$$M_i = \sqrt{\left(M_i^x\right)^2 + \left(M_i^y\right)^2 + \left(M_i^z\right)^2}$$

and the relative angles between neighboring spins are immediately available. In the calculation, we found that the magnetization is almost independent of the sites. For simplicity, hereafter we show only the overall magnetization M, which is obtained by averaging over all the M_i within one

TABLE I. E_b and M_0 obtained by various methods are shown for comparison. SB, CC, SWT, VMC, FN, and FNE denote Schwinger boson mean field theory, coupled cluster, spin-wave theory, variational Monte Carlo, fixed node, and fixed node with effective Hamiltonian, respectively. For the three CC references, the maximal parameters n used in the lattice-animal-based subsystem (LSUBn) scheme are listed and indicated by superscript $(*)$, while, for the other methods, the maximal lattice sizes used in the calculations are summarized. For almost all the finite-size calculations listed here, the estimated results are obtained by polynomial extrapolation with respect to either lattice size or the LSUB parameter.

Method	E_b	M_0	Year	Max. size
This work	−0.18334(10)	0.161(5)	2020	∞
SB+1/N [30]		0.224	2018	432
DMRG [29]	−0.1837 (7)		2016	
CC [28]	−0.1838	0.21535	2016	10^*
SB [26]		0.2739	2015	∞
SWT [26]		0.2386	2015	∞
SE [26]		0.198(34)	2015	∞
CC [27]	−0.18403(7)	0.198(5)	2015	10^*
CC [24]	−0.1843	0.1865	2014	10^*
VMC [25]	−0.18163(7)	0.2715(30)	2014	324
SWT [26]	−0.18228	0.24974	2009	∞
VMC [22]	−0.18233(3)	0.265	2009	576
DMRG [16]		0.205(15)	2007	~140
FN [17]	−0.17996(1)	0.1625(30)	2006	324
FNE [17]	−0.18062(2)	0.1765(35)	2006	324
SE [21]	−0.18340(13)	0.19(2)	2006	∞
VMC [19]	−0.1773(3)	0.36	2006	108
ED [13]	−0.1842	0.193	2004	36
DMRG [20]	−0.1814		2001	144
GFMC [15]	−0.18193(3)	0.205(10)	1999	144

unit cell. Similar to the calculation of E_b, for a given D, we extrapolate M as a function of $1/\chi$ to the infinite χ limit.

The results for D from 7 to 13 are illustrated in Fig. 4. We notice that, for $D = 9$, our result is already smaller than most recent results; see Table I. Clearly, it shows that M decreases roughly as a monotonic function of $1/D$. To get a more accurate estimate, we try to fit them with two typical formulas. One is a power-law formula, i.e., $M = M_0 + a \times (1/D)^b$, yielding $M_0 = 0.161$. The other is an exponential formula, i.e., $M = M_0 + a \times \exp(-bD)$, with $M_0 = 0.164$ for the best fit.

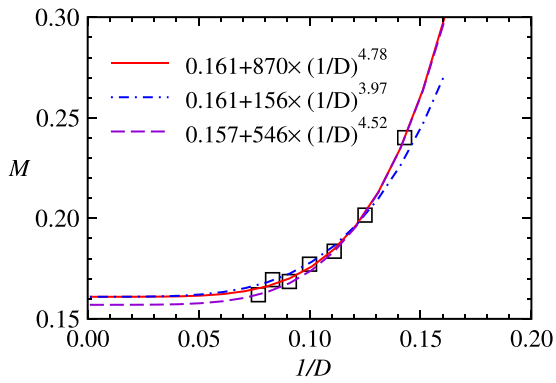

FIG. 4. M, marked as □, is plotted as a function of $1/D$. All the data points have already been extrapolated to the infinite-χ limit. The lines are different numerical fittings: solid line is obtained from all D, while dot-dashed line and dashed line are obtained from even and odd D only, respectively.

TABLE II. Angles (in unit of degree) of the magnetization vectors between nearest neighbors are shown. Location of the upward triangles in the unit cell is listed explicitly. x, y, and z are the three directions in the triangle lattice, as marked in Fig. 1. They indicate the corresponding bonds of the triangle here.

	$D = 4, \chi = 32$			$D = 13, \chi = 170$		
(μ, ν)	x	y	z	x	y	z
(1, 1)	120.004	120.000	119.996	120.010	119.988	120.002
(1, 2)	119.999	120.000	120.001	119.985	119.994	120.021
(1, 3)	119.997	120.000	120.003	120.005	119.993	120.002
(2, 1)	120.004	120.000	119.996	120.005	120.012	119.983
(2, 2)	119.999	120.000	120.001	119.992	120.013	119.994
(2, 3)	119.997	120.000	120.003	120.004	120.013	119.983
(3, 1)	120.004	120.000	119.006	120.003	120.001	119.996
(3, 2)	119.999	120.000	120.001	119.993	120.993	119.986
(3, 3)	119.997	120.000	120.003	120.004	119.994	120.998

With a careful inspection of Fig. 4, we notice that there is a tiny even-odd oscillation in the magnetization as a function of D, which suggests we fit the magnetization for even and odd D separately. Using the power-law formula, we obtain $M_0 = 0.161$ and $M_0 = 0.157$ for even and odd D, respectively. Defining the error bar as the standard deviation among the four different M_0 obtained above, we conclude that $M_0 = 0.161(5)$, which is very close to the lower bound obtained by SE [21,26]. One may notice that this value is also very close to that in Ref. [17], but their ground-state energy is obviously not optimal. More details can be found in Table I.

We would like to emphasize that the magnetization we obtained is slightly smaller than 1/3 of its classical value. In particular, it is smaller than all that obtained in previous works. On one hand, such a small magnetization requires a careful finite-size analysis to obtain a quantitatively reliable estimation in numerical calculations such as the ED, DMRG, and Monte Carlo. On the other hand, generally, the TNS method usually tends to overestimate the magnetization in frustrated systems when D is finite [40]. This suggests that probably our smallest result for finite D is the upper bound of the magnetization. Therefore, it is quite likely that M_0 has been overestimated in previous works.

In Table II, we present the data of the angles between all the nearest neighbors in the unit cell, for two sets of parameters, i.e., $D = 4$ with $\chi = 32$ and $D = 13$ with $\chi = 170$. It shows that (I) the 120° angles between nearest neighbors are almost perfect, in the sense that the largest error bar is as small as 0.021° with D up to 13, and (II) in contrast to the magnetization, the angles are almost independent of D and χ, as long as they are not too small. Therefore, we can safely conclude the existence of the TMO.

C. Larger unit cell

The result of TNS simulation might also depend on the size of the unit cell; thus we need to check whether the unit cell we

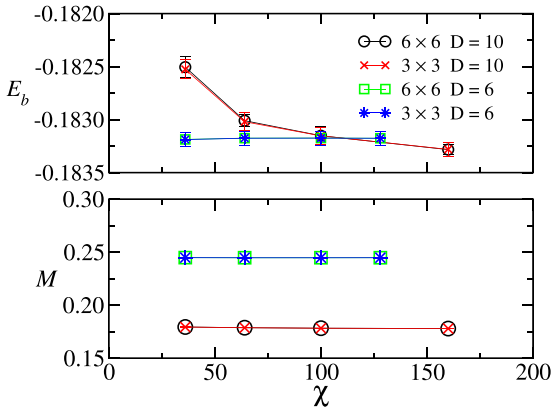

FIG. 5. E_b and M are shown as a function of χ for 6×6 and 3×3 unit cells. Our results show that they agree well, suggesting that the 3×3 unit cell is large enough for TAHM.

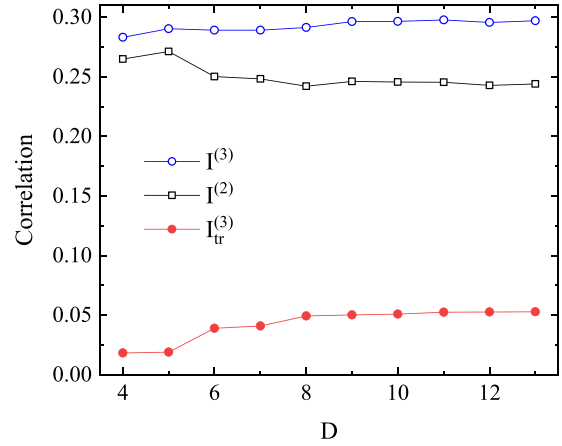

FIG. 6. Correlation measured by mutual information in one triangle of the ground-state wave function. Here, $I^{(2)}$ denotes the total pair correlation, namely $I^{(2)} = I_{ab} + I_{bc} + I_{ca}$. See Eqs. (8) and (9).

used in the wave function ansatz is sufficiently large. For this purpose, we compare our results from the 3×3 unit cell with those from the 6×6 unit cell. In Fig. 5, we plot E_b and M as a function of χ for $D = 10$ and 6. The data is in excellent agreement for the two different unit cells and the differences at all data points are negligible compared to the error bar. This suggests that the 3×3 unit cell in our work is already large enough for TAHM.

D. Many-body correlation

The motivation to study the many-body correlation in this model comes from two perspectives. On one hand, the existence of TMO indicates that in each triangle there is probably some three-body correlation that is essentially different from the two-body correlation. Actually, this is one reason why we use the PESS ansatz to study this model. On the other hand, from the view of quantum information, for mixed many-body states, generally the total correlation leaks more information than the part peculiar to quantum states only, i.e., entanglement, which has no classical counterpart [52]. Moreover, though PESS is believed to be able to capture the many-body correlation better, there is no direct numerical evidence yet to demonstrate the existence of such correlation in the obtained wave function. Therefore, the frustrated TAHM offers such an opportunity to study the many-body correlation, especially the three-body correlation in a triangle.

To be specific, we envisage that the three spins $\{\sigma_a, \sigma_b, \sigma_c\}$ in a triangle comprise a mixed quantum state, which can be characterized by the reduced-density matrix $\rho^{(3)}$ defined below:

$$\rho^{(3)}_{II'} = \sum_J |\Psi_{IJ}\rangle\langle\Psi_{I'J}|, \tag{7}$$

where I denotes the composite index $\{\sigma_a, \sigma_b, \sigma_c\}$ and J represents all the rest spins. Similarly we can define $\rho^{(1)}$ for one spin and $\rho^{(2)}$ for a pair of spins sharing one bond.

Once the three kinds of mixed states are defined, we can calculate the von Neumann entropies, $S = -\mathrm{Tr}\rho \ln \rho$, for these states. For simplicity, we use S_i, S_{ij}, and S_{ijk} to denote the entropies corresponding to spin σ_i, spin pair $\{\sigma_i, \sigma_j\}$, and spin simplex $\{\sigma_i, \sigma_j, \sigma_k\}$, respectively, with $i, j, k = a, b, c$. Then we measure the correlations in this small triangle through the following quantities defined below:

$$\begin{aligned} I_a &= S_a, \\ I_{ab} &= S_a + S_b - S_{ab}, \\ I^{(3)} &= S_a + S_b + S_c - S_{abc}, \end{aligned} \tag{8}$$

where I_{ab} and $I^{(3)}$ are the two-body and three-body mutual information which are used to measure the total correlation for a general quantum system [52], respectively. Other terms can be obtained similarly. Moreover, the true tripartite correlation $I^{(3)}_{tr}$, which is more relevant in this context, can be identified from $I^{(3)}$ by excluding the pair correlation contributions, i.e.,

$$I^{(3)}_{tr} = I^{(3)} - I_{ab} - I_{bc} - I_{ca}. \tag{9}$$

The obtained results are shown in Fig. 6. We can see clearly that in this frustrated system, as D becomes larger, pair correlation becomes weaker, while simplex correlation becomes stronger. More importantly, it shows that, as D increases, the true tripartite correlation $I^{(3)}_{tr}$ becomes more and more significant, which coincides with the fact that the TMO can be argued to have imposed a global constraint on the three spins simultaneously, not just a local constraint on each pair in the triangle. This makes us more confident that the ground state should be of TMO and that the PESS wave function can indeed grasp well the many-body correlation in this model.

IV. SUMMARY

In summary, using tensor-network algorithms with a PESS-type trial wave function, we have studied the spin-1/2 antiferromagnetic Heisenberg model on the triangular lattice. This wave function was optimized by the simple update imaginary-time evolution method and the expectation values were estimated by the multisublattice CTMRG algorithm. By comparing the ground-state energy to that in other works, we confirmed that the wave function converges to the ground state and it is a TMO state. In particular, the

magnetization is $M_0 = 0.161(5)$, which is smaller than that reported in previous calculations like GFMC and DMRG. Although frustration and quantum fluctuation do introduce some unusual properties into the model, such as rotonlike excitations [21], its ground state remains magnetically ordered. This result is consistent with the correlation analysis, which shows that, as D increases, the two-body correlation becomes weaker gradually, while the three-body correlation becomes increasingly significant. In view of the experience that the TNS method, especially when simple update strategy is used, may tend to overestimate the magnetization of frustrated systems a little bit for a finite D (as evidenced by the comparison for $D = 6$ in the main text, for example), we believe that our work provides benchmark results for this model.

ACKNOWLEDGMENTS

We are supported by the National R&D Program of China (Grants No. 2017YFA0302900 and No. 2016YFA0300503), the National Natural Science Foundation of China (Grants No. 11874188, No. 12047501, No. 11834005, and No. 11774420), and by the Research Funds of Renmin University of China (Grant No. 20XNLG19). We thank H.-J. Liao and H.-Y. Zou for helpful discussions about automatic differentiation and PEPS calculations.

Q.L. and H.L. contributed equally to this work.

[1] P. W. Anderson, Mater. Res. Bull. **8**, 153 (1973).
[2] P. W. Anderson, Science **235**, 4793 (1987).
[3] F. Mila, Eur. J. Phys. **21**, 499 (2000).
[4] Y. Zhou, K. Kanoda, and T. K. Ng, Rev. Mod. Phys. **89**, 025003 (2017).
[5] L. Savary and L. Balents, Rep. Prog. Phys. **80**, 016502 (2017).
[6] P. A. Lee, Science **321**, 1306 (2008).
[7] L. Balents, Nature (London) **464**, 199 (2010).
[8] D. A. Huse and V. Elser, Phys. Rev. Lett. **60**, 2531 (1988).
[9] D. Yoshioka and J. Miyazaki, J. Phys. Soc. Jpn. **60**, 614 (1991).
[10] L. O. Manuel, A. E. Trumper, and H. A. Ceccatto, Phys. Rev. B **57**, 8348 (1998).
[11] H. Nishimori and H. Nakanishi, J. Phys. Soc. Jpn. **57**, 626 (1988).
[12] B. Bernu, P. Lecheminant, C. Lhuillier, and L. Pierre, Phys. Rev. B **50**, 10048 (1994).
[13] J. Richter, J. Schulenburg, A. Honecker, and D. Schmalfuß, Phys. Rev. B **70**, 174454 (2004).
[14] N. Suzuki, F. Matsubara, S. Fujiki, and T. Shirakura, Phys. Rev. B **90**, 184414 (2014).
[15] L. Capriotti, A. E. Trumper, and S. Sorella, Phys. Rev. Lett. **82**, 3899 (1999).
[16] S. R. White and A. L. Chernyshev, Phys. Rev. Lett. **99**, 127004 (2007).
[17] S. Yunoki and S. Sorella, Phys. Rev. B **74**, 014408 (2006).
[18] S. A. Kulagin, N. Prokofev, O. A. Starykh, B. Svistunov, and C. N. Varney, Phys. Rev. Lett. **110**, 070601 (2013).
[19] C. Weber, A. Laüchli, F. Mila, and T. Giamarchi, Phys. Rev. B **73**, 014519 (2006).
[20] T. Xiang, J. Lou, and Z. Su, Phys. Rev. B **64**, 104414 (2001).
[21] W. Zheng, J. O. Fjærestad, R. R. P. Singh, R. H. McKenzie, and R. Coldea, Phys. Rev. B **74**, 224420 (2006).
[22] D. Heidarian, S. Sorella, and F. Becca, Phys. Rev. B **80**, 012404 (2009).
[23] A. L. Chernyshev and M. E. Zhitomirsky, Phys. Rev. B **79**, 144416 (2009); Erratum, *ibid.* **91**, 219905(E) (2015).
[24] D. J. J. Farnell, O. Götze, J. Richter, and R. F. Bishop, and P. H. Y. Li, Phys. Rev. B **89**, 184407 (2014).
[25] R. Kaneko, S. Morita, and M. Imada, J. Phys. Soc. Jpn. **83**, 093707 (2014).
[26] E. A. Ghioldi, A. Mezio, L. O. Manuel, R. R. P. Singh, J. Oitmaa, and A. E. Trumper, Phys. Rev. B **91**, 134423 (2015).
[27] P. H. Y. Li, R. F. Bishop, and C. E. Campbell, Phys. Rev. B **91**, 014426 (2015).
[28] O. Götze, J. Richter, R. Zinke, and D. J. J. Farnell, J. Magn. Magn. Mater. **397**, 333 (2016).
[29] Y. Iqbal, W.-J. Hu, R. Thomale, D. Poilblanc, and F. Becca, Phys. Rev. B **93**, 144411 (2016).
[30] E. A. Ghioldi, M. G. Gonzalez, S.-S. Zhang, Y. Kamiya, L. O. Manuel, A. E. Trumper, and C. D. Batista, Phys. Rev. B **98**, 184403 (2018).
[31] H. D. Zhou, E. S. Choi, G. Li, L. Balicas, C. R. Wiebe, Y. Qiu, J. R. D. Copley, and J. S. Gardner, Phys. Rev. Lett. **106**, 147204 (2011).
[32] Y. Li and Q. Zhang, J. Phys.: Condens. Matter **25**, 026003 (2013).
[33] H. Niggemann and J. Zittarz, Z. Phys. B: Condens. Matter **101**, 289 (1996); H. Niggemann, A. Klmper, and J. Zittartz, *ibid.* **104**, 103 (1997).
[34] T. Nishino, Y. Hieida, K. Okunishi, N. Maeshima, Y. Akutsu, and A. Gendiar, Prog. Theor. Phys. **105**, 409 (2001).
[35] F. Verstraete and J. I. Cirac, arXiv:cond-mat/0407066; J. I. Cirac, D. Perez-Garcia, N. Schuch, and F. Verstraete, Rev. Mod. Phys. **93**, 045003 (2021).
[36] S. Montangero, *Introduction to Tensor Network Methods* (Springer, New York, 2018).
[37] R. Orus, Ann. Phys. (NY) **349**, 117 (2014); Eur. Phys. J. B **87**, 280 (2014); Nat. Rev. Phys. **1**, 538 (2019).
[38] H. C. Jiang, R. R. P. Singh, and L. Balents, Phys. Rev. Lett. **111**, 107205 (2013).
[39] P. Corboz, T. M. Rice, and M. Troyer, Phys. Rev. Lett. **113**, 046402 (2014).
[40] H. J. Liao, Z. Y. Xie, J. Chen, Z. Y. Liu, H. D. Xie, R. Z. Huang, B. Normand, and T. Xiang, Phys. Rev. Lett. **118**, 137202 (2017).
[41] Z. Y. Xie, J. Chen, M. P. Qin, J. W. Zhu, L. P. Yang, and T. Xiang, Phys. Rev. B **86**, 045139 (2012).
[42] C. Wang, S. M. Qin, and H. J. Zhou, Phys. Rev. B **90**, 174201 (2014).
[43] M. Friesdorf, A. H. Werner, W. Brown, V. B. Scholz, and J. Eisert, Phys. Rev. Lett. **114**, 170505 (2015).
[44] F. Verstraete and J. I. Cirac, Phys. Rev. Lett. **104**, 190405 (2010).

[45] Y. Z. Liu, Y. Meurice, M. P. Qin, J. Unmuth-Yockey, T. Xiang, Z. Y. Xie, J. F. Yu, and H. Y. Zou, Phys. Rev. D **88**, 056005 (2013).
[46] A. Tilloy and J. I. Cirac, Phys. Rev. X **9**, 021040 (2019).
[47] Z. Y. Han, J. Wang, H. Fan, L. Wang, and P. Zhang, Phys. Rev. X **8**, 031012 (2018).
[48] Z. F. Gao, S. Cheng, R. Q. He, Z. Y. Xie, H. H. Zhao, Z. Y. Lu, and T. Xiang, Phys. Rev. Research **2**, 023300 (2020).
[49] Z. Y. Xie, J. Chen, J. F. Yu, X. Kong, B. Normand, and T. Xiang, Phys. Rev. X **4**, 011025 (2014).
[50] T. Nishino and K. Okunishi, J. Phys. Soc. Jpn. **65**, 891 (1996).
[51] R. Orús and G. Vidal, Phys. Rev. B **80**, 094403 (2009).
[52] B. Zeng, X. Chen, D. L. Zhou, and X. G. Wen, *Quantum Information Meets Quantum Matter* (Springer, New York, 2019).
[53] G. Vidal, Phys. Rev. Lett. **98**, 070201 (2007).
[54] H. C. Jiang, Z. Y. Weng, and T. Xiang, Phys. Rev. Lett. **101**, 090603 (2008).
[55] M. Lubasch, J. I. Cirac, and M. C. Banuls, Phys. Rev. B **90**, 064425 (2014).
[56] B. B. Chen, Y. Gao, Y. B. Guo, Y. Liu, H. H. Zhao, H. J. Liao, L. Wang, T. Xiang, W. Li, and Z. Y. Xie, Phys. Rev. B **101**, 220409(R) (2020); H. J. Liao, J. G. Liu, L. Wang, and T. Xiang, Phys. Rev. X **9**, 031041 (2019).
[57] The full update and automatic differentiation were performed with environment bond dimension $\chi = 50$, and the result was roughly converged for $D = 6$.
[58] Z. Y. Xie, H. J. Liao, R. Z. Huang, H. D. Xie, J. Chen, Z. Y. Liu, and T. Xiang, Phys. Rev. B **96**, 045128 (2017).
[59] Though the decorated square lattice ansatz is not a good ansatz for triangular lattice due to the likely threefold rotational symmetry breaking, we have not tried the PEPS ansatz defined on the original triangular lattice because of the extremely high cost, since coordination number there is 6 which is too large for tensor-network calculations.